ROYAL SOCIETY
OF CHEMISTRY

## PAPER

Check for updates

# HOMER: a reparameterization of the harmonic oscillator model of aromaticity (HOMA) for excited states†

Enrique M. Arpa [ID] * and Bo Durbeej [ID] *

Excited-state aromaticity (ESA) and antiaromaticity (ESAA) are by now well-established concepts for explaining photophysical properties and photochemical reactivities of cyclic, conjugated molecules. However, their application is less straightforward than the corresponding process by which the thermal chemistry of such systems is rationalized in terms of ground-state aromaticity (GSA) and antiaromaticity (GSAA). Recognizing that the harmonic oscillator model of aromaticity (HOMA) provides an easy way to measure aromaticity on geometric grounds, it is therefore notable that this model is yet to be parameterized for excited states. Against this background, we here present a new parameterization of HOMA – termed HOMER – for the $T_1$ state of both carbocyclic and heterocyclic compounds based on high-level quantum-chemical calculations. Considering CC, CN, NN and CO bonds and testing the parametrization using calculated magnetic data as reference, we find that the description of ESA and ESAA by HOMER is superior to that afforded by the original HOMA scheme, and that it reaches the same overall quality as HOMA does for GSA and GSAA. Furthermore, we demonstrate that the derived HOMER parameters can be used for predictive modeling of ESA and ESAA at very different levels of theory. Altogether, the results highlight the potential of HOMER to facilitate future studies of ESA and ESAA.

## 1. Introduction

Despite the undisputed role of aromaticity in shaping the structures and controlling the chemical reactivities of cyclic, conjugated π-electron systems, a precise definition of this concept and a general approach to directly quantify aromaticity are elusive.[1–5] In principle, the reason for this situation is the lack of a quantum-mechanical operator that would make aromaticity a proper observable and, therefore, amenable to direct experimental measurement.[5] Consequently, aromaticity is usually probed in an indirect fashion by calculating or measuring a physicochemical property that reflects its manifestation[4] and relates to, *e.g.*, induced ring currents, energetic stabilization or electron delocalization.[5] For example, the ability of NMR spectroscopy to detect diamagnetic ring currents in aromatic compounds through their effect (downfield) on proton chemical shifts[6] is the basis for the calculation of nucleus-independent chemical shift (NICS) indices.[7,8] In the isomerization stabilization energy (ISE) approach, in turn, the energetic

stabilization associated with aromaticity is quantified in terms of the energy difference between a methylated derivative of the aromatic system at hand and its non-aromatic, exocyclic methylene isomer.[9] Other indices, such as the *para*-delocalization (PDI),[10] aromatic fluctuation (FLU)[11] and multicenter (MCI)[12] ones, probe aromaticity based on different measures of electron delocalization.[13]

Besides magnetism-, energy- and electron delocalization-based measures, there are also geometry-based aromaticity indices that rely on the typical characteristic of aromatic systems to show equalization of bond lengths.[14,15] Of these models, perhaps the most effective is the harmonic oscillator model of aromaticity (HOMA).[14–16] Originally developed for carbocyclic π-electron systems, this model assumes that the energy required to extend/compress a carbon–carbon (CC) bond in such a system depends quadratically on the extension/compression relative to the equilibrium bond length.[16] Under this assumption, the original HOMA index was defined as

$$\text{HOMA} = 1 - \frac{\alpha}{n} \sum_i (R_i - R_{\text{opt}})^2, \qquad (1)$$

where the summation runs over all CC bonds in the carbocycle considered, $n$ is the number of CC bonds, and $R_i$ are the calculated or experimentally determined CC bond lengths. Furthermore, as for the two parameters ($R_{\text{opt}}$ and $\alpha$), $R_{\text{opt}}$ is

*Division of Theoretical Chemistry, IFM, Linköping University, SE-581 83 Linköping, Sweden. E-mail: enrique.arpa@liu.se, bodur@ifm.liu.se*

This journal is © the Owner Societies 2023

*Phys. Chem. Chem. Phys.*, 2023, **25**, 16763–16771 | 16763

the optimal CC bond length achieved by a fully aromatic system whose HOMA value is 1 on account of all $R_i$ being equal to $R_{opt}$, and $\alpha$ is a normalization factor determined in such a way that the HOMA value is 0 for a model non-aromatic system. Defining $R_{opt}$ as the length at which the energy needed to extend the bond to a "pure" single bond equals the energy needed to compress it to a "pure" double bond, using the CC bond lengths in ethane and ethylene to represent pure single and double bonds, and assuming the ratio of force constants for such bonds to be $1:2$, the initial estimate of $R_{opt}$ (1.397 Å) in 1972[16] is very close to the experimental value of 1.398 Å subsequently obtained for benzene by neutron diffraction at 15 K.[17] Moreover, by setting HOMA = 0 in eqn (1), this estimate was then used to obtain a value of $\alpha$ as

$$\alpha = \frac{2}{\left(R_S - R_{opt}\right)^2 + \left(R_D - R_{opt}\right)^2}, \qquad (2)$$

where $R_S$ and $R_D$ are the lengths of the pure single and double CC bonds in ethane and ethylene.[16]

Perhaps the most appealing feature of the HOMA index is the ease with which its values can be obtained,[18,19] requiring only information about molecular geometry ($R_i$) that oftentimes is accessible from both experiments and quantum-chemical calculations. Throughout the years, various extensions of the original model have been proposed.[20–24] In 1993, Krygowski[20] made it applicable to heterocyclic $\pi$-electron systems by introducing a modified HOMA index as

$$\text{HOMA} = 1 - \frac{\alpha_{XY}}{n} \sum_i \left(R_{XY,i} - R_{XY,opt}\right)^2, \qquad (3)$$

where the summation runs over all $n$ bonds in the cyclic structure and a bond between atoms X and Y are assigned $R_{opt}$ and $\alpha$ values that are specific for that type of bond. As in the 1972 study,[16] these values were determined using experimental bond lengths of suitable references systems for each type of bond considered (CC, CN, NN, CO, CP, CS and NO), but with 1,3-butadiene now replacing ethane and ethylene for CC bond lengths.[20] In later research, other parameterizations of the HOMA index have been reported where the reference bond lengths are derived from quantum-chemical calculations rather than from experiments,[22] or are selected from other sources of experimental data.[23]

The HOMA index also has a few well-known shortcomings, such as its tendency to exaggerate aromatic character in cases where bonds have similar lengths,[14] which by itself clearly is not a sufficient sign of aromaticity. Furthermore, by relying on parameterization, it is less broadly applicable than many of the other indices mentioned above. For example, because of the need of model aromatic/non-aromatic/antiaromatic reference systems from which to derive suitable $R_{opt}$ and $\alpha$ parameters, HOMA has not yet been applied to aromatic all-metal clusters[25,26] in the same way that electron delocalization-based indices have.[27] Additionally, there are both positive[28] and negative[29] results on the ability of HOMA to describe changes in aromatic character along a reaction path.

So far, our presentation has pertained to different ways to probe aromaticity and antiaromaticity in the electronic ground state ($S_0$), i.e., to ground-state aromaticity (GSA) and anti-aromaticity (GSAA). However, already in 1972, following earlier work by Dewar[30] and Zimmerman,[31] the concepts of excited-state aromaticity (ESA) and antiaromaticity (ESAA)[32–36] were given a solid theoretical foundation through the discovery by Baird[37] that annulenes with $4n$ and $4n + 2$ $\pi$-electrons are respectively aromatic and antiaromatic in their lowest triplet $\pi\pi^*$ excited state ($T_1$), thus implying a reversal of (anti)aromatic character in this state relative to the ground state as asserted by Hückel's rule. With time, and particularly since the past decade or so,[38,39] ESA and ESAA have established themselves as very useful concepts for explaining and predicting photophysical properties[40–43] and photochemical reactivities[28,44–56] of both triplet and singlet excited states of organic molecules.

A major hurdle for the use of the ESA and ESAA concepts as tools in rational design in photophysics and photochemistry is that conventional experimental measurements (by, e.g., NMR spectroscopy and X-ray crystallography) required to probe aromaticity are much more difficult to perform for molecules in an excited state,[35] although developments in time-resolved spectroscopy and electron diffractometry have proven to offer new possibilities in this regard.[35,45] As a result, most studies on ESA and ESAA to date have relied on the possibility to calculate aromaticity indices using quantum-chemical methods. Nevertheless, this is generally more challenging for excited states than for ground states, as the former (especially singlet excited states) call for more elaborate modeling and because there is a relative lack of benchmark data for assessing how well different indices measure ESA and ESAA[57] (the accuracy of different indices for GSA and GSAA, on the other hand, has been thoroughly investigated[13,58–61]).

In this light, it is of particular interest to establish how the HOMA index performs for excited states, as this index is probably the easiest to calculate, requiring only a quantum-chemical geometry optimization. Indeed, for this reason, HOMA has often been employed to highlight photochemical consequences of ESA and ESAA,[28,45–47,49,52–54] despite that it is yet to be parameterized for excited states. Against this background, we here present a parameterization of HOMA for the $T_1$ state of both carbocyclic and heterocyclic compounds (throughout this work, the "$T_1$ state" refers to the lowest-lying $^3\pi\pi^*$ state). Terming the parameterization as the Harmonic Oscillator Model of Excited-state aRomaticity (HOMER) and considering CC, CN, NN and CO bonds (which are the most abundant sources of $\pi$-conjugation in heterocyclic compounds[62]), its performance is tested for a set of 28 molecules across a large portion of the aromatic–antiaromatic spectrum. Thereby, it is found that HOMER offers a vast improvement over standard parameterizations of HOMA[20] in the description of ESA and ESAA, as judged from a comparison of how well the two indices correlate with calculated NICS values, which are widely considered as among the most dependable measures of aromaticity and antiaromaticity.[60,63] Furthermore, by the same token, it is demonstrated that HOMER is about as accurate for ESA and

16764 | Phys. Chem. Chem. Phys., 2023, 25, 16763–16771

This journal is © the Owner Societies 2023

ESAA as HOMA is for GSA and GSAA. Altogether, these findings pave the way for the use of HOMER to probe ESA and ESAA by means of geometry optimizations.

## 2. Results and discussion

### 2.1. Parameterization of HOMER

In the same way that benzene is the $S_0$ aromatic reference system for the application of HOMA to carbocyclic compounds, our parameterization of HOMER requires selecting a suitable $T_1$ aromatic reference system for determining the $R_{opt}$ value for each bond included in the parameterization (*i.e.*, CC, CN, NN and CO). Here, for the CC bond, $T_1$ cyclobutadiene was chosen as reference, which is natural given Karadakov's demonstration that cyclobutadiene, which is antiaromatic in $S_0$, becomes square-symmetric and aromatic in $T_1$,[33] in line with Baird's original prediction for $4n$ $\pi$-electron systems.[37] For the same reason, the parameterization of CN, NN and CO bonds made use of the $T_1$ aza- and oxo-analogues of cyclobutadiene shown in Fig. 1, which only contain CN, NN or CO bonds in their rings. In order to obtain as accurate $R_{opt}$ parameters as possible for the different bonds, the $T_1$ geometries of cyclobutadiene and its aza- and oxo-analogues were optimized with the gold standard[64,65] *ab initio* multiconfigurational complete active space second-order perturbation theory (CASPT2) method[66] in combination with the large cc-pVQZ basis set.[67] Since each individual bond type XY was parameterized according to

$$\text{HOMER} = 1 - \frac{\alpha_{XY}}{n} \sum_i (R_{XY,i} - R_{XY,opt})^2, \qquad (4)$$

these reference systems will have HOMER values of exactly 1 at this level of theory and are considered to be fully $T_1$ aromatic.

Besides selecting $T_1$ aromatic reference systems for determining the $R_{opt}$ parameters, it is also necessary to choose appropriate references systems for deriving the corresponding $\alpha$ parameters employed by HOMER. Here, rather than using model non-aromatic systems (as HOMA does[14–16]), we invoked model $T_1$ antiaromatic systems for this task. Specifically, following the well-known result that benzene changes character from aromatic in $S_0$ to antiaromatic in $T_1$,[33,37] the different bonds were parameterized based on $T_1$ benzene and the $T_1$ aza- and oxo-analogues of benzene, which also are shown in Fig. 1 and only contain CN, NN or CO bonds in their rings. By optimizing the $T_1$ geometries of these reference systems,

**Table 1** HOMER parameters for different bonds and the corresponding 1993 HOMA parameters

| Bond | HOMER | | HOMA[a] | |
|------|----------------------|----------------------|----------------------|----------------------|
| | $R_{opt}$ (Å) | $\alpha$ (Å$^{-2}$) | $R_{opt}$ (Å) | $\alpha$ (Å$^{-2}$) |
| CC | 1.437 | 950.74 | 1.388 | 257.70 |
| CN | 1.390 | 506.43 | 1.334 | 93.52 |
| NN | 1.375 | 187.36 | 1.309 | 130.33 |
| CO | 1.379 | 164.96 | 1.265 | 157.38 |

[a] Values taken from ref. [20].

using again CASPT2/cc-pVQZ, the $\alpha$ parameters for the different bonds were obtained from the condition that

$$\frac{\alpha_{XY}}{n} \sum_i (R_{XY,i} - R_{XY,opt})^2 = 2, \qquad (5)$$

where $R_{XY,i}$ are the resulting CC/CN/NN/CO bond lengths. Accordingly, the reference systems will have HOMER values of exactly −1 at this level of theory and are taken to be fully $T_1$ antiaromatic. It should be pointed out that while the $R_{opt}$ parameters of both HOMA and HOMER are derived with the intention that both indices approach 1 in the case of strong aromaticity, the $\alpha$ parameters of HOMA and HOMER are obtained with somewhat different goals. Namely, for HOMA, the goal is that the HOMA value is close to 0 for a model non-aromatic system, whereas for HOMER, the goal is that the HOMER value is close to −1 for a model antiaromatic system. By symmetry, then, the HOMER value for a non-aromatic system is expected to be close to 0. The results of the parameterization of HOMER are summarized in Table 1.

### 2.2. Probing GSA and GSAA with HOMA

Before assessing the description of ESA and ESAA by HOMER, it is necessary to first test how well HOMA performs for GSA and GSAA, as reference. To this end, the 1993 parameterization of HOMA[20] (see eqn (3) and Table 1) was used to probe the aromatic character of the 28 compounds shown in Fig. 2, which cover a large portion of the aromatic-antiaromatic spectrum and comprise four-, five- and six-membered carbocyclic and N,O-heterocyclic species with different substitution patterns. The underlying calculations (*i.e.*, the $S_0$ geometry optimizations) were carried out with the CASPT2 method[66] and a medium-sized basis set – cc-pVDZ[67] – that represents a typical choice for such calculations. The performance of HOMA was evaluated based on a comparison with $S_0$ NICS$_{zz}$ values (corresponding to the $zz$-component of the magnetic shielding tensor[8]) calculated with the complete active space self-consistent field (CASSCF) method[68] and the same basis set (cc-pVDZ) that was used to obtain HOMA values. Besides calculating NICS$_{zz}$ values at 1 Å distances above the geometric centers of the rings (NICS$_{zz}(1)$), which is a proven approach,[8] distances of 0 (NICS$_{zz}(0)$) and 2 Å (NICS$_{zz}(2)$) were also considered, so as to minimize bias in the comparison of HOMA and NICS values. In addition to testing HOMA in this way, the same exact approach was also used to assess the potency of HOMER in describing GSA and GSAA. Here, however, it should be kept in mind that HOMER is
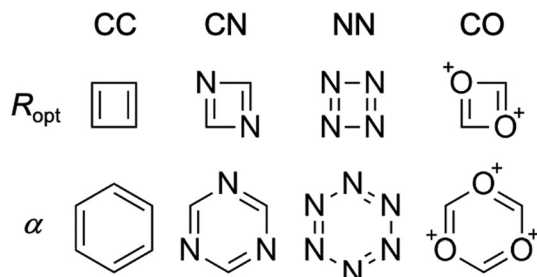


**Fig. 1** Reference systems used for the parameterization of HOMER.

This journal is © the Owner Societies 2023

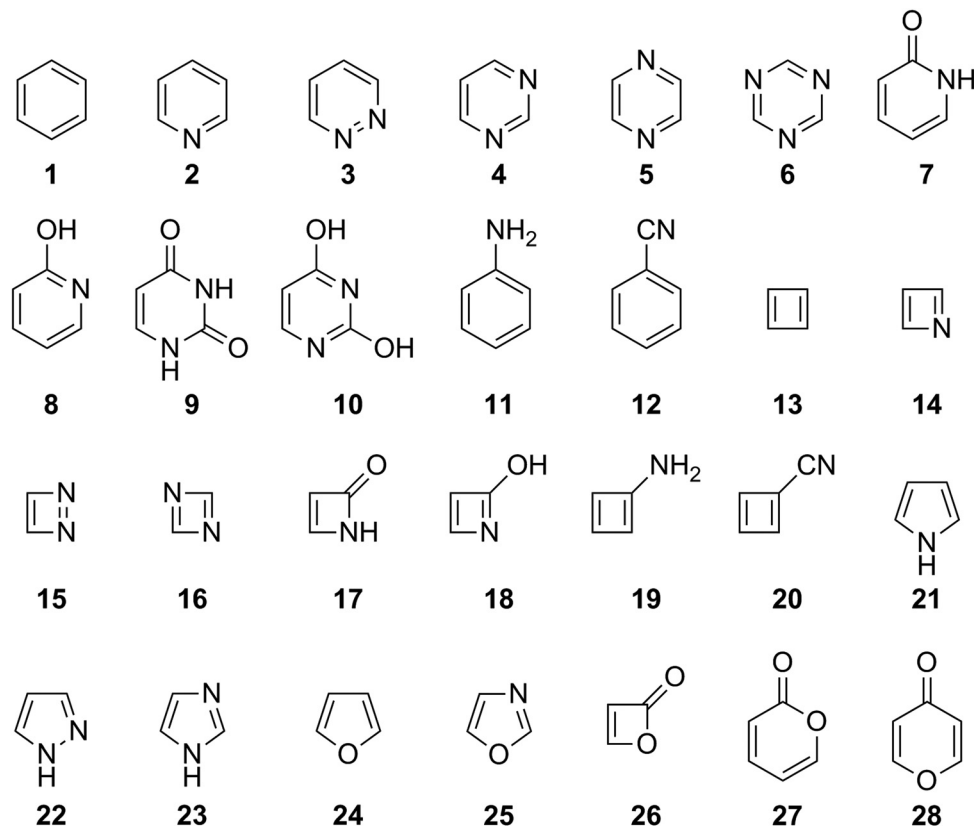*Phys. Chem. Chem. Phys.*, 2023, **25**, 16763–16771 | **16765**

Fig. 2 Compounds used to assess the performance of the HOMA and HOMER indices.

parameterized for ESA and ESAA. Also, for the sake of accuracy, the parameterization is based on geometries optimized with the CASPT2 method, with which NICS values cannot be calculated. Instead, NICS values are calculated with the closest possible method to CASPT2, which is CASSCF.

Before going through the results of the calculations, it should be noted that HOMA and HOMER on the one hand and NICS on the other reflect different properties of an aromatic system (the static geometry and the response to a magnetic field, respectively). However, this does not mean that it is inappropriate to use NICS as reference in evaluating the performance of HOMA and HOMER. Contrarily, given the multidimensional character of the aromaticity concept, such an approach is even desirable, and good correlations between HOMA and NICS have indeed been documented in numerous studies of many different compounds.[1,14,69–72] Here, it may also be emphasized that this work is primarily concerned with assessing the relative performance of HOMA and HOMER, for which the different origins of HOMA/HOMER and NICS are expected to be a minor issue, rather than the absolute performance of either index relative to NICS.

The results of the calculations are presented in Fig. 3, which uses the $NICS_{zz}(1)$ values for comparing HOMA and HOMER with NICS. For both comparisons, the correlation between the two sets of data was quantified by the $R^2$ value resulting from a linear regression analysis. The corresponding results obtained with the $NICS_{zz}(0)$ and $NICS_{zz}(2)$ values as reference are given in
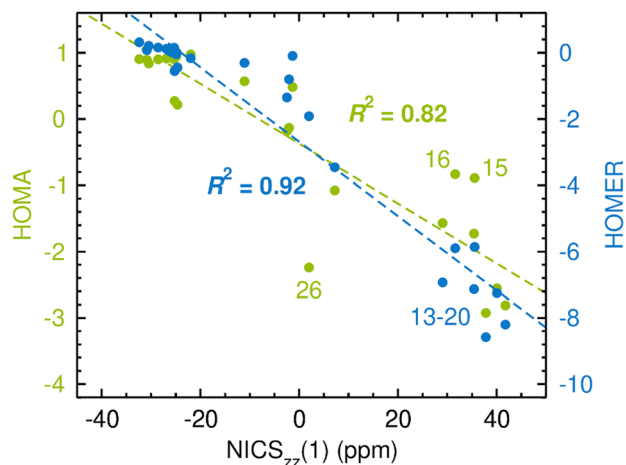


Fig. 3 Correlation between CASPT2-based HOMA (in green font)/ HOMER (in blue font) values and CASSCF-based $NICS_{zz}(1)$ values in probing GSA and GSAA. The data points for some compounds deserving particular attention are highlighted by their numbers according to Fig. 2.

Fig. S1 and S3, respectively, in the ESI.† Furthermore, all raw data underlying these analyses are summarized in Table S1 in the ESI.† From Fig. 3, it is clear that HOMA on the whole agrees quite well with NICS, showing an $R^2$ value of 0.82 (the $R^2$ values relative to the $NICS_{zz}(0)$ and $NICS_{zz}(2)$ data are of similar magnitude, 0.75 and 0.84, see Fig. S1 and S3, ESI†). Hence, in line with many previous studies,[1,14,69–72] the easily calculable

16766 | Phys. Chem. Chem. Phys., 2023, 25, 16763–16771

This journal is © the Owner Societies 2023

HOMA index appears to be a viable alternative to the dependable[60,63] but more elaborate NICS index in probing GSA and GSAA, which well motivates the goal of the present work to parameterize HOMER for the description of ESA and ESAA. Notably, the most prominent HOMA outliers in Fig. 3 (compounds **15**, **16** and **26**), whose exclusion from the analysis would increase the $R^2$ value from 0.82 to 0.93, are all four-membered heterocyclic species. Accordingly, it could well be that such species pose a special challenge for HOMA, although the three other of them among the 28 test systems (compounds **14**, **17** and **18**) follow the overall HOMA/NICS correlation much more closely. Another possibility is that the NICS values of either **15**/**16** or **26** are skewed by a ring-size dependence. Still, because of its local nature, NICS is generally found to exhibit a modest ring-size dependence.[7,72] This is in contrast to global magnetic aromaticity indices, such as those based on magnetic susceptibilities, which show a pronounced ring-size dependence.[7,72]

As an aside, it is striking in Fig. 3 that HOMER actually achieves a better correlation with NICS ($R^2 = 0.92$) than HOMA does ($R^2 = 0.82$), despite that HOMER is parameterized exclusively for ESA and ESAA. While this may be a coincidence, it could also reflect an advantage in our approach to employ cyclic, aromatic and antiaromatic compounds in deriving the $R_{opt}$ and $\alpha$ parameters of HOMER, as opposed to using noncyclic, non-aromatic systems, as done in the 1993 parameterization of HOMA.[20] At the same time, it should be noted that the HOMER values for GSA and GSAA are somewhat wayward, being, for example, much more negative than $-1$ for the antiaromatic compounds **13–20**. This means that while HOMER provides a surprisingly balanced assessment of GSA and GSAA in a series of different molecules, its value for an individual molecule should not be taken as a quantitative measure of the GSA or GSAA in that system without comparison with the values for a few related molecules.

### 2.3. Probing ESA and ESAA with HOMER

Having tested the performance of HOMA for GSA and GSAA, we turn next to the assessment of how well HOMER describes ESA and ESAA. This part of the work was carried out in a completely analogous fashion as the previous part, except that the CASPT2 geometry optimizations and the CASSCF NICS calculations were now done for the $T_1$ state of the 28 compounds in Fig. 2. The results of the assessment, including a parallel test of HOMA, are given in Fig. 4, with $NICS_{zz}(1)$ values as reference. The corresponding results obtained with $NICS_{zz}(0)$ and $NICS_{zz}(2)$ values as reference are presented in Fig. S1 and S3 (ESI†), respectively, and all raw data for the analyses are summarized in Table S2 in the ESI.† Before going through the results, it should be noted that HOMA and HOMER, by considering relaxed $T_1$ geometries, cannot describe the aromatic character of the $T_1$ state in the vertically excited Franck–Condon region. As a consequence, if an antiaromatic $T_1$ state is formed upon vertical excitation, this antiaromaticity might be reduced by the geometric relaxation.

From Fig. 4, it is firstly apparent that HOMA does not correlate at all with NICS ($R^2 < 0.01$), which is also the case
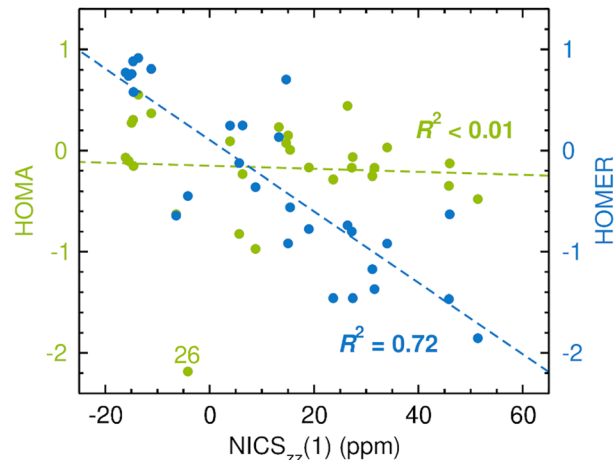


Fig. 4 Correlation between CASPT2-based HOMA (in green font)/HOMER (in blue font) values and CASSCF-based $NICS_{zz}(1)$ values in probing ESA and ESAA.

when the comparison is made with the $NICS_{zz}(0)$ (see Fig. S1, ESI†) or $NICS_{zz}(2)$ (see Fig. S3, ESI†) data. Hence, using HOMA with standard parameters[20] to probe variations in ESA and ESAA between different molecules does not yield reliable results. HOMER, on the other hand, fares much better, achieving a correlation with an $R^2$ value of 0.72 (the $R^2$ values relative to the $NICS_{zz}(0)$ and $NICS_{zz}(2)$ data are quite comparable, 0.57 and 0.69, see Fig. S1 and S3, ESI†). Accordingly, our parameterization of HOMER appears to have been successful and seemingly offers a means to measure ESA and ESAA that is about as consistent with NICS calculations as HOMA is for measuring GSA and GSAA (see Fig. 2).

Interestingly, further scrutiny of the results in Fig. 4 reveals that both the HOMA and the HOMER $R^2$ values increase if lactones (compounds **26** and **27**) and lactams (compounds **7**, **9** and **17**) are excluded from the analysis (the HOMER $R^2$ value increases from 0.72 to 0.81). In fact, as can be seen in Table 2, a similar effect is observed for all correlations tested up to this point. Thus, the rather complex electronic features shown by many ester and amide bonds[73] may require a more specific model than those afforded by the 1993 parameterization of HOMA[20] or the present parameterization of HOMER. Designing such models is beyond the scope of this work. Of the five lactone/lactam compounds, the most prominent HOMA outlier in Fig. 4 is **26**, a four-membered lactone. Since we have already seen that a common characteristic of the three HOMA outliers

Table 2 $R^2$ values for the correlations between CASPT2-based HOMA/HOMER values and CASSCF-based $NICS_{zz}(1)$ values obtained with and without lactones/lactams included in the analysis

| Index | Probing of | $R^2$ with lactones/lactams | $R^2$ without lactones/lactams |
|---|---|---|---|
| HOMA | GSA and GSAA | 0.82 | 0.90 |
| HOMER | GSA and GSAA | 0.92 | 0.97 |
| HOMA | ESA and ESAA | <0.01 | 0.12 |
| HOMER | ESA and ESAA | 0.72 | 0.81 |

This journal is © the Owner Societies 2023

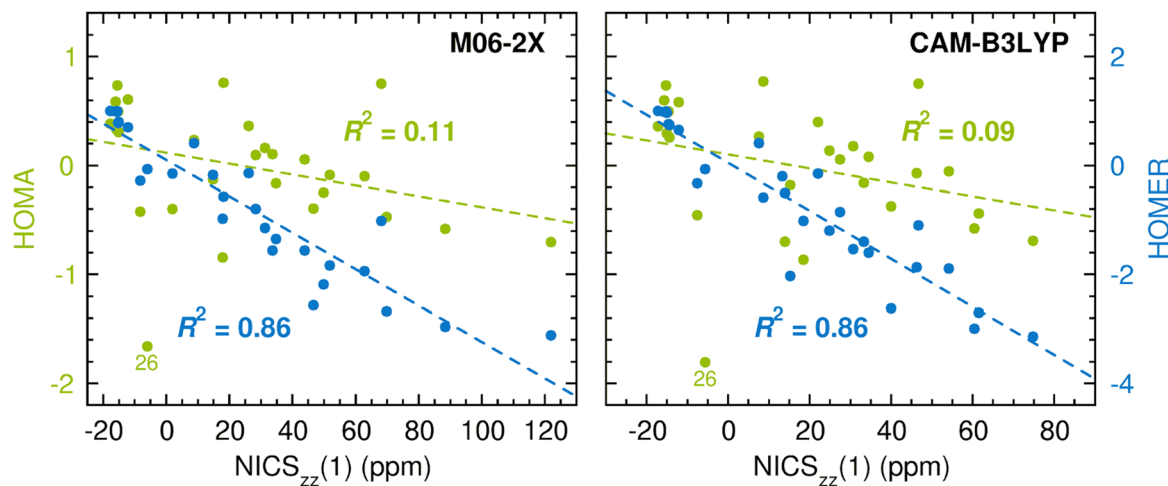*Phys. Chem. Chem. Phys.*, 2023, **25**, 16763–16771 | **16767**

Fig. 5 Correlation between DFT-based HOMA (in green font)/HOMER (in blue font) values and DFT-based $NICS_{zz}(1)$ values in probing ESA and ESAA.

in Fig. 3 (**15**, **16** and **26**) is that they are four-membered rings, the behavior of **26** in Fig. 4 may stem from an enhancement of complex ester bonding by the four-membered ring.

As noted in the Introduction, a main advantage of geometry-based aromaticity indices is that their values are easy to derive once atomic-level resolution structures of the compounds of interest have been obtained, either experimentally or computationally. Up to this point, the performance of HOMER has been tested based on geometries optimized with the CASPT2 method.[66] The reason for using CASPT2 for this task is its status as a highly accurate method[64,65] that is generally applicable to both ground and excited states, owing to the inclusion of both static and dynamic electron correlation. At the same time, CASPT2 is an expensive method with many subtleties, which means that it is yet to be adopted as a workhorse by non-experts in the field. Instead, for many years, this role has been played by density functional theory (DFT) methods, which offer a much more favorable cost-performance ratio and are easier to use. In this light, we decided to also test HOMER for the description of ESA and ESAA based on geometries and $NICS_{zz}(1)$ values for the $T_1$ state of the **28** compounds calculated with M06-2X[74] and CAM-B3LYP,[75] which are two popular hybrid density functionals of different types. These results are presented in Fig. 5. The corresponding results testing HOMA for the description of GSA and GSAA are given in Fig. S4 and S5, respectively, in the ESI.† Furthermore, all raw data for the calculations are summarized in Tables S3 and S4 (M06-2X) and in Tables S5 and S6 (CAM-B3LYP) in the ESI.†

Notably, the DFT results in Fig. 5 fully corroborate the previous CASPT2/CASSCF results in Fig. 4 by showing that HOMER ($R^2 = 0.86$) enables a considerably more reliable measurement of ESA and ESAA than HOMA ($R^2 = 0.09$–0.11). In fact, the HOMER $R^2$ values of 0.86 are even better than that of 0.72 assigned to the calculations in Fig. 4, despite that HOMER was parameterized through CASPT2 calculations. Moreover, the HOMER $R^2$ values are virtually identical to those of 0.85–0.86 in Fig. S4 and S5 (ESI†) that quantify how well HOMA measures GSA and GSAA at the DFT level. Given that the

$T_1$ geometry optimizations were carried out using unrestricted DFT (UDFT), it is also pleasing to note from Table S7 in the ESI† that the geometries and HOMER values for the **28** compounds obtained at the UM06-2X level are generally close to those instead obtained with M06-2X in the framework of time-dependent DFT (TD-DFT).[76] Altogether, these results show that HOMER can also be used successfully at other levels of theory than that employed for the parameterization, which is a very appealing characteristic in terms of applicability (but has been considered difficult to achieve by HOMA-related aromaticity indices[77]). Thus, while this work has focused on small molecular systems, it will be worthwhile in future studies to test the HOMER parameters derived herein also for molecular systems of varying sizes, using levels of theory of varying sophistication.

## 3. Conclusions

In summary, recognizing the need for an easily calculable, geometric measure of ESA and ESAA, we have presented a parameterization of the HOMA index for application to the $T_1$ state of both carbocyclic and heterocyclic compounds, which we term HOMER (the Harmonic Oscillator Model of Excited-state aRomaticity). Focusing on CC, CN, NN and CO bonds, the corresponding $R_{opt}$ and $\alpha$ parameters are derived from high-level *ab initio* (CASPT2/cc-pVQZ) calculations on cyclic, model $T_1$ aromatic and antiaromatic systems, rather than from experimental bond lengths of non-cyclic, non-aromatic systems (which is the more common procedure in the development of HOMA-related aromaticity indices). Collecting suitable reference data by calculating $S_0$ and $T_1$ $NICS_{zz}$ values for a panel of 28 small molecules across the aromatic-antiaromatic spectrum, the quality of the parameterization is assessed by quantifying its correlation with these $NICS_{zz}$ values, and by comparing this correlation with that achieved by the 1993 parameterization of HOMA.[20] Thereby, it is found that while HOMA cannot reliably describe variations in ESA and ESAA between different molecules, the good performance of HOMER at the same task is fully

**16768** | *Phys. Chem. Chem. Phys.*, 2023, **25**, 16763–16771

This journal is © the Owner Societies 2023

comparable to that HOMA contrarily shows when used to probe variations in GSA and GSAA. Moreover, by employing both *ab initio* and cheaper DFT methods in the assessment, another important result that further paves the way for HOMER in studies of ESA and ESAA is the observation that the *ab initio* $R_{opt}$ and $\alpha$ parameters can be used for predictive calculations at very different levels of theory. Indeed, this will facilitate the future application of HOMER to larger molecular systems than those considered herein. Besides such applications, another worth-while extension of the present work would be to test how well these parameters, derived here for the $T_1$ state, describe ESA and ESAA in the $S_1$ state. For the sake of generality, one would of course hope that the parameters can be used for *all* low-lying excited states of organic molecules, regardless of their spin multiplicity. If this is not possible, then a specific parameterization for the $S_1$ state is certainly feasible, as model compounds that are aromatic/non-aromatic/antiaromatic in this state are readily available.[33]

## 4. Computational methods

All calculations except where otherwise noted were done with the medium-sized cc-pVDZ basis set.[67] All CASPT2 calculations were carried out based on CASSCF reference wave functions optimized with active spaces including only $\pi$ and $\pi^\star$ orbitals, which correspond to (4,4), (6,5) and (6,6) active spaces for compounds with four-, five- and six-membered rings, respectively.

The CASPT2 $T_1$ geometry optimizations performed to derive the $R_{opt}$ and $\alpha$ parameters of HOMER were done with the large cc-pVQZ basis set[67] and using convergence criteria that are considerably tighter (maximum component of the gradient vector: 0.00001 hartree bohr$^{-1}$; maximum component of the displacement vector: 0.00004 bohr; maximum energy change: 0.000001 hartree) than the default ones in the BAGEL 1.1.2 software[78] employed for these calculations.

The CASPT2 $S_0$ and $T_1$ geometry optimizations performed to assess HOMA and HOMER relative to NICS were done using the default convergence criteria in BAGEL 1.1.2. Based on the resulting geometries, HOMA and HOMER values were calculated with the Multiwfn 3.7 software,[79] employing a standard version (with the 1993 HOMA parameters[20]) for the former and a modified version (with our derived HOMER parameters) for the latter. These values were compared with NICS$_{zz}$ values[8] calculated from CASSCF $S_0$ and $T_1$ wave functions with the Dalton 2016.2 software,[80,81] using gauge-including atomic orbitals and the aforementioned (4,4), (6,5) and (6,6) active spaces for compounds with four-, five- and six-membered rings, respectively.

The complementary $S_0$ and $T_1$ geometry optimizations that were performed to also compare HOMA and HOMER with NICS at the DFT level were carried out with the M06-2X[74] and CAM-B3LYP[75] hybrid density functionals, using UDFT for the $T_1$ state. Furthermore, in control calculations, $T_1$ geometries and HOMER values were also derived through TD-M06-2X optimizations. All DFT calculations were done with the Gaussian 16

software.[82] Again, the associated HOMA and HOMER values were obtained with the use of standard (HOMA) and modified (HOMER) versions of Multiwfn 3.7. As for the corresponding DFT NICS$_{zz}$ values, finally, they too were calculated by employing gauge-including atomic orbitals.

As for frequency calculations at the optimized geometries, it should first be noted that *all* $S_0$ and $T_1$ geometries considered in this work were optimized to be planar, because such structures are the ideal ones for assessing aromaticity and anti-aromaticity. For any given geometry, the corresponding frequency calculation was always performed at the same level of theory used to optimize the geometry in question. At the CASPT2 (DFT) level, the frequency calculations were carried out numerically (analytically) with BAGEL 1.1.2 (Gaussian 16). Thereby, all $S_0$ geometries were found to be potential-energy minima with real vibrational frequencies only. For some of the 28 compounds used to assess the performance of HOMA and HOMER, the corresponding $T_1$ geometries were found to be first-order saddle points with one imaginary vibrational frequency. Importantly, this has no bearing on the evaluation of ESA or ESAA by HOMA and HOMER, which can be done as long as the geometries in question are stationary points (which they are).

## Conflicts of interest

There are no conflicts to declare.

## Acknowledgements

## References

1 T. M. Krygowski, M. K. Cyrański, Z. Czarnocki, G. Häfelinger and A. R. Katritzky, *Tetrahedron*, 2000, **56**, 1783–1796.

2 P. V. R. Schleyer, *Chem. Rev.*, 2001, **101**, 1115–1118.

3 A. T. Balaban, D. C. Oniciu and A. R. Katritzky, *Chem. Rev.*, 2004, **104**, 2777–2812.

4 M. Solà, *Front. Chem.*, 2017, **5**, 22.

5 M. Solà, *WIREs Comput. Mol. Sci.*, 2019, **9**, e1404.

6 R. H. Mitchell, *Chem. Rev.*, 2001, **101**, 1301–1315.

7 P. V. R. Schleyer, C. Maerker, A. Dransfeld, H. Jiao and N. J. R. van Eikema Hommes, *J. Am. Chem. Soc.*, 1996, **118**, 6317–6318.

8 H. Fallah-Bagher-Shaidaei, C. S. Wannere, C. Corminboeuf, R. Puchta and P. V. R. Schleyer, *Org. Lett.*, 2006, **8**, 863–866.

This journal is © the Owner Societies 2023

*Phys. Chem. Chem. Phys.*, 2023, **25**, 16763–16771 | **16769**

9 P. V. R. Schleyer and F. Pühlhofer, *Org. Lett.*, 2002, **4**, 2873–2876.

10 J. Poater, X. Fradera, M. Duran and M. Solà, *Chem. – Eur. J.*, 2003, **9**, 400–406.

11 E. Matito, M. Duran and M. Solà, *J. Chem. Phys.*, 2005, **122**, 014109.

12 P. Bultinck, R. Ponec and S. van Damme, *J. Phys. Org. Chem.*, 2005, **18**, 706–718.

13 F. Feixas, E. Matito, J. Poater and M. Solà, *Chem. Soc. Rev.*, 2015, **44**, 6434–6451.

14 T. M. Krygowski and M. K. Cyrański, *Chem. Rev.*, 2001, **101**, 1385–1419.

15 T. M. Krygowski, H. Szatylowicz, O. A. Stasyuk, J. Dominikowska and M. Palusiak, *Chem. Rev.*, 2014, **114**, 6383–6422.

16 J. Kruszewski and T. M. Krygowski, *Tetrahedron Lett.*, 1972, **13**, 3839–3842.

17 G. A. Jeffrey, J. R. Ruble, R. K. McMullan and J. A. Pople, *Proc. R. Soc. London, Ser. A*, 1987, **414**, 47–57.

18 J. C. Dobrowolski, *ACS Omega*, 2019, **4**, 18699–18710.

19 H. Szatylowicz, P. A. Wieczorkiewicz and T. M. Krygowski, in *Aromaticity: Modern Computational Methods and Applications*, ed. I. Fernández, Elsevier, 2021, pp. 71–99.

20 T. M. Krygowski, *J. Chem. Inf. Comput. Sci.*, 1993, **33**, 70–78.

21 T. M. Krygowski and M. K. Cyrański, *Tetrahedron*, 1996, **52**, 1713–1722.

22 E. D. Raczyńska, M. Hallman, K. Kolczyńska and T. M. Stępniewski, *Symmetry*, 2010, **2**, 1485–1509.

23 C. P. Frizzo and M. A. P. Martins, *Struct. Chem.*, 2012, **23**, 375–380.

24 R. Kalescky, E. Kraka and D. Cremer, *J. Phys. Chem. A*, 2014, **118**, 223–237.

25 A. I. Boldyrev and L.-S. Wang, *Chem. Rev.*, 2005, **105**, 3716–3757.

26 F. Feixas, E. Matito, J. Poater and M. Solà, *WIREs Comput. Mol. Sci.*, 2013, **3**, 105–122.

27 F. Feixas, E. Matito, M. Duran, J. Poater and M. Solà, *Theor. Chem. Acc.*, 2011, **128**, 419–431.

28 J. Wang, B. Oruganti and B. Durbeej, *ChemPhotoChem*, 2019, **3**, 450–460.

29 E. Matito, J. Poater, M. Duran and M. Solà, *THEOCHEM*, 2005, **727**, 165–171.

30 M. J. S. Dewar, *Tetrahedron*, 1966, **8**, 75–92.

31 H. E. Zimmermann, *J. Am. Chem. Soc.*, 1996, **88**, 1564–1565.

32 P. Wan and E. Krogh, *J. Chem. Soc., Chem. Commun.*, 1985, 1207–1208.

33 P. B. Karadakov, *J. Phys. Chem. A*, 2008, **112**, 7303–7309.

34 H. Ottosson, *Nat. Chem.*, 2012, **4**, 969–971.

35 J. Oh, Y. M. Sung, Y. Hong and D. Kim, *Acc. Chem. Res.*, 2018, **51**, 1349–1358.

36 L. J. Karas and J. I. Wu, *Nat. Chem.*, 2022, **14**, 719–727.

37 N. C. Baird, *J. Am. Chem. Soc.*, 1972, **94**, 4941–4948.

38 M. Rosenberg, C. Dahlstrand, K. Kilså and H. Ottosson, *Chem. Rev.*, 2014, **114**, 5379–5425.

39 J. Kim, J. Oh, A. Osuka and D. Kim, *Chem. Soc. Rev.*, 2022, **51**, 268–292.

40 B. J. Lampkin, Y. H. Nguyen, P. B. Karadakov and B. VanVeller, *Phys. Chem. Chem. Phys.*, 2019, **21**, 11608–11614.

41 K. J. Fallon, P. Budden, E. Salvadori, A. M. Ganose, C. N. Savory, L. Eyre, S. Dowland, Q. Ai, S. Goodlett, C. Risko, D. O. Scanlon, C. W. M. Kay, A. Rao, R. H. Friend, A. J. Musser and H. Bronstein, *J. Am. Chem. Soc.*, 2019, **141**, 13867–13876.

42 O. El Bakouri, J. R. Smith and H. Ottosson, *J. Am. Chem. Soc.*, 2020, **142**, 5602–5617.

43 H. Kim, W. Park, Y. Kim, M. Filatov, C. H. Choi and D. Lee, *Nat. Commun.*, 2021, **12**, 5409.

44 L. Gutiérrez-Arzaluz, F. Cortés-Guzmán, T. Rocha-Rinza and J. Peón, *Phys. Chem. Chem. Phys.*, 2015, **17**, 31608–31612.

45 M. Hada, S. Saito, S. Tanaka, R. Sato, M. Yoshimura, K. Mouri, K. Matsuo, S. Yamaguchi, M. Hara, Y. Hayashi, F. Röhricht, R. Herges, Y. Shigeta, K. Onda and R. J. D. Miller, *J. Am. Chem. Soc.*, 2017, **139**, 15792–15800.

46 B. Oruganti, J. Wang and B. Durbeej, *Org. Lett.*, 2017, **19**, 4818–4821.

47 B. Durbeej, J. Wang and B. Oruganti, *ChemPlusChem*, 2018, **83**, 958–967.

48 T. Yamakado, S. Takahashi, K. Watanabe, Y. Matsumoto, A. Osuka and S. Saito, *Angew. Chem. Int. Ed.*, 2018, **57**, 5438–5443.

49 J. Toldo, O. El Bakouri, M. Solà, P.-O. Norrby and H. Ottosson, *ChemPlusChem*, 2019, **84**, 712–721.

50 C.-H. Wu, L. J. Karas, H. Ottosson and J. I. Wu, *Proc. Natl. Acad. Sci. U. S. A.*, 2019, **116**, 20303–20308.

51 L. J. Karas, C.-H. Wu, H. Ottosson and J. I. Wu, *Chem. Sci.*, 2020, **11**, 10071–10077.

52 B. Oruganti, P. P. Kalapos, V. Bhargav, G. London and B. Durbeej, *J. Am. Chem. Soc.*, 2020, **142**, 13941–13953.

53 R. Kotani, L. Liu, P. Kumar, H. Kuramochi, T. Tahara, P. Liu, A. Osuka, P. B. Karadakov and S. Saito, *J. Am. Chem. Soc.*, 2020, **142**, 14985–14992.

54 E. M. Arpa and B. Durbeej, *Phys. Chem. Chem. Phys.*, 2022, **24**, 11496–11500.

55 B. Oruganti, J. Wang and B. Durbeej, *J. Org. Chem.*, 2022, **87**, 11565–11571.

56 J. Yan, T. Slanina, J. Bergman and H. Ottosson, *Chem. – Eur. J.*, 2023, **29**, e202203748.

57 J. Pedersen and K. V. Mikkelsen, *J. Phys. Chem. A*, 2023, **127**, 122–130.

58 F. Feixas, E. Matito, J. Poater and M. Solà, *J. Comput. Chem.*, 2008, **29**, 1543–1554.

59 M. Solà, F. Feixas, J. O. C. Jiménez-Halla, E. Matito and J. Poater, *Symmetry*, 2010, **2**, 1156–1179.

60 R. Gershoni-Poranne and A. Stanger, *Chem. Soc. Rev.*, 2015, **44**, 6597–6615.

61 J. Pedersen and K. V. Mikkelsen, *RSC Adv.*, 2022, **12**, 2830–2842.

62 N. N. Makhova, L. I. Belen'kii, G. A. Gazieva, I. G. Dalinger, L. S. Konstantinova, V. V. Kuznetsov, A. N. Kravchenko, M. M. Krayushkin, O. A. Rakitin, A. M. Starosotnikov, L. L. Fershtat, S. A. Shevelev, V. Z. Shirinian and V. N. Yarovenko, *Russ. Chem. Rev.*, 2020, **89**, 55–124.

63 A. Stanger, *Eur. J. Org. Chem.*, 2020, 3120–3127.

64 M. Schreiber, M. R. Silva-Junior, S. P. A. Sauer and W. Thiel, *J. Chem. Phys.*, 2008, **128**, 134110.

**16770** | *Phys. Chem. Chem. Phys.*, 2023, **25**, 16763–16771

This journal is © the Owner Societies 2023

65 Š. Budzák, G. Scalmani and D. Jacquemin, *J. Chem. Theory Comput.*, 2017, **13**, 6237–6252.

66 K. Andersson, P.-Å. Malmqvist and B. O. Roos, *J. Chem. Phys.*, 1992, **96**, 1218–1226.

67 T. H. Dunning Jr., *J. Chem. Phys.*, 1989, **90**, 1007–1023.

68 B. O. Roos, P. R. Taylor and P. E. M. Siegbahn, *Chem. Phys.*, 1980, **48**, 157–173.

69 M. K. Cyrański and T. M. Krygowski, *Tetrahedron*, 1998, **54**, 14919–14924.

70 M. K. Cyrański and T. M. Krygowski, *Tetrahedron*, 1999, **55**, 6205–6210.

71 M. K. Cyrański, B. T. Stępień and T. M. Krygowski, *Tetrahedron*, 2000, **56**, 9663–9667.

72 Z. Chen, C. S. Wannere, C. Corminboeuf, R. Puchta and P. V. R. Schleyer, *Chem. Rev.*, 2005, **105**, 3842–3888.

73 C. R. Kemnitz and M. J. Loewen, *J. Am. Chem. Soc.*, 2007, **129**, 2521–2528.

74 Y. Zhao and D. G. Truhlar, *Theor. Chem. Acc.*, 2008, **120**, 215–241.

75 T. Yanai, D. P. Tew and N. C. Handy, *Chem. Phys. Lett.*, 2004, **393**, 51–57.

76 M. E. Casida and M. Huix-Rotllant, *Annu. Rev. Phys. Chem.*, 2012, **63**, 287–323.

77 M. Andrzejak, P. Kubisiak and K. K. Zborowski, *Struct. Chem.*, 2013, **24**, 1171–1184.

78 T. Shiozaki, *WIREs Comput. Mol. Sci.*, 2018, **8**, e1331.

79 T. Lu and F. Chen, *J. Comput. Chem.*, 2012, **33**, 580–592.

80 K. Aidas, C. Angeli, K. L. Bak, V. Bakken, R. Bast, L. Boman, O. Christiansen, R. Cimiraglia, S. Coriani, P. Dahle, E. K. Dalskov, U. Ekström, T. Enevoldsen, J. J. Eriksen, P. Ettenhuber, B. Fernández, L. Ferrighi, H. Fliegl, L. Frediani, K. Hald, A. Halkier, C. Hättig, H. Heiberg, T. Helgaker, A. C. Hennum, H. Hettema, E. Hjertenæs, S. Høst, I.-M. Høyvik, M. F. Iozzi, B. Jansik, H. J. A. Jensen, D. Jonsson, P. Jørgensen, J. Kauczor, S. Kirpekar, T. Kjærgaard, W. Klopper, S. Knecht, R. Kobayashi, H. Koch, J. Kongsted, A. Krapp, K. Kristensen, A. Ligabue, O. B. Lutnæs, J. I. Melo, K. V. Mikkelsen, R. H. Myhre, C. Neiss, C. B. Nielsen, P. Norman, J. Olsen, J. M. H. Olsen, A. Osted, M. J. Packer, F. Pawlowski, T. B. Pedersen, P. F. Provasi, S. Reine, Z. Rinkevicius, T. A. Ruden, K. Ruud, V. Rybkin, P. Salek, C. C. M. Samson, A. Sánchez de Merás, T. Saue, S. P. A. Sauer, B. Schimmelpfennig, K. Sneskov, A. H. Steindal, K. O. Sylvester-Hvid, P. R. Taylor, A. M. Teale, E. I. Tellgren, D. P. Tew, A. J. Thorvaldsen, L. Thøgersen, O. Vahtras, M. A. Watson, D. J. D. Wilson, M. Ziolkowski and H. Ågren, *WIREs Comput. Mol. Sci.*, 2014, **4**, 269–284.

81 Dalton A Molecular Electronic Structure Program, Release Dalton 2016.2, 2016, **https://daltonprogram.org** (accessed February 10, 2023).

82 M. J. Frisch, G. W. Trucks, H. B. Schlegel, G. E. Scuseria, M. A. Robb, J. R. Cheeseman, G. Scalmani, V. Barone, G. A. Petersson, H. Nakatsuji, X. Li, M. Caricato, A. V. Marenich, J. Bloino, B. G. Janesko, R. Gomperts, B. Mennucci, H. P. Hratchian, J. V. Ortiz, A. F. Izmaylov, J. L. Sonnenberg, D. Williams-Young, F. Ding, F. Lipparini, F. Egidi, J. Goings, B. Peng, A. Petrone, T. Henderson, D. Ranasinghe, V. G. Zakrzewski, J. Gao, N. Rega, G. Zheng, W. Liang, M. Hada, M. Ehara, K. Toyota, R. Fukuda, J. Hasegawa, M. Ishida, T. Nakajima, Y. Honda, O. Kitao, H. Nakai, T. Vreven, K. Throssell, J. A. Montgomery Jr., J. E. Peralta, F. Ogliaro, M. J. Bearpark, J. J. Heyd, E. N. Brothers, K. N. Kudin, V. N. Staroverov, T. A. Keith, R. Kobayashi, J. Normand, K. Raghavachari, A. P. Rendell, J. C. Burant, S. S. Iyengar, J. Tomasi, M. Cossi, J. M. Millam, M. Klene, C. Adamo, R. Cammi, J. W. Ochterski, R. L. Martin, K. Morokuma, O. Farkas, J. B. Foresman and D. J. Fox, *Gaussian 16, Revision C.01*, Gaussian, Inc., Wallingford CT, 2016.

This journal is © the Owner Societies 2023

*Phys. Chem. Chem. Phys.*, 2023, **25**, 16763–16771 | **16771**